ACS APPLIED MATERIALS & INTERFACES

www.acsami.org

Research Article

# Spontaneous Creation of Anisotropic Polymer Crystals with Orientation-Sensitive Birefringence in Liquid Drops

Weichao Shi,* Xiaotong Chen, Baihui Li, and David A. Weitz

Cite This: https://dx.doi.org/10.1021/acsami.9b17308

Read Online

ACCESS | Metrics & More | Article Recommendations | Supporting Information

**ABSTRACT:** It remains a grand challenge to prepare anisotropic crystal superstructures with sensitive optical properties in polymer science and materials field. This study demonstrates that semicrystalline polymers develop into anisotropic hollow spherulitic crystals spontaneously at interfaces of liquid drops. In contrast to conventional spherulites with centrosymmetric optics and grain boundaries, these anisotropic spherulitic crystals have vanished boundary defects, tunable aspect ratios, and noncentrosymmetric, orientation-sensitive birefringence. The experimental finding is elaborated in poly(L-lactic acid) crystals and is further verified in a broad class of semicrystalline polymers, irrespective of molecular chirality, chemical constitution, or interfacial modification. The facile methods and general mechanism revealed in this study shed light on developing new types of optical microdevices and synthesis of anisotropic semicrystalline particles from liquid emulsions.

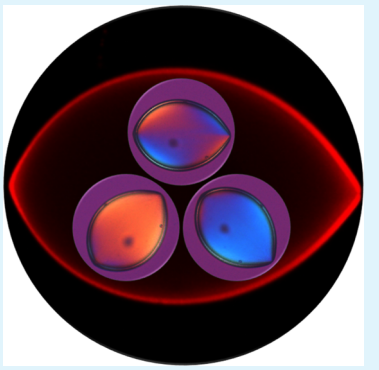

**KEYWORDS:** *microfluidics, anisotropic hollow spherulite, birefringence, liquid/liquid interfaces, semicrystalline polymer*



## INTRODUCTION

Anisotropic crystal structures provide orientation-sensitive optical properties, which are broadly used as optical devices in printing, chemical sensing, and biosensing.[1−5] The fast growth in materials' demand provides a great opportunity for semicrystalline polymers, which cover about two-thirds of total polymer species.[6] For crystallization of polymer random coils, single crystals of polymer sheets can be created in dilute solutions. Those single crystal sheets are essentially anisotropic in shape and optical properties.[6,7] In concentrated polymer solutions or melts, however, polymer crystal sheets are initiated from a nucleation site and grow isotropically in 3D. The crystallized structure finally develops into a spherical organization, namely, spherulites.[8,9] The centrosymmetric geometry of spherulites makes the optical properties orientation-insensitive.[6−13] Moreover, a spherulite may impinge on other spherulites nearby, which creates grain boundaries between them. The grain boundaries are defect-rich regions and are detrimental to optical behaviors. Thus, preparing anisotropic crystal superstructures without macroscopic defects has remained a grand challenge in polymer science and materials field for decades.[14,15]

A general strategy to prepare anisotropic crystals is in liquid drops. A liquid drop usually maintains a spherical shape by interfacial tension. To generate anisotropy, various physical or chemical methods are applied to overcome the interfacial tension. The physical methods include using mechanical shear, magnetic field, electric field, etc.[16−18] For example, liquid crystal drops can be deformed to long stripes under an electric field.[18] The chemical methods use chemical reactions or reagents to tune the interfacial tension.[19−22] Hawker's group used amphiphilic surfactants to control the assembly of diblock copolymers and prepared stripped, ellipsoidal particles as photonic crystals.[19,20] Those methods either require additional energy input or are limited for special chemical components.

An additional bottleneck with crystallization in liquid drops is still the defect. Li's group found that polymer crystals grown in miniemulsions generate curved nanocrystals with significant defects.[23,24] Similar problems are reported in colloids and liquid crystal drops. Colloid crystals develop with grain boundary scars or macroscopic voids on curved interfaces.[25−27] Topological defects, such as defect dipoles or even quadrupoles, are inevitable in nematic liquid crystal drops.[28,29]

In addressing those challenges, here, we show that polymer crystallization at interfaces of liquid drops creates anisotropic hollow spherulites spontaneously without chemical or physical treatments. The anisotropic crystallized morphology can be well modulated, and grain boundaries vanish to a point when only one spherulite is created in the drop. The anisotropic hollow spherulites provide noncentrosymmetric, orientation-sensitive optical properties. Our findings could be applied to a broad class of semicrystalline polymer materials, irrespective of polymer constitutions. The fundamental understanding sheds light on the polymer crystallization mechanism at liquid/liquid

Received: September 24, 2019
Accepted: December 23, 2019

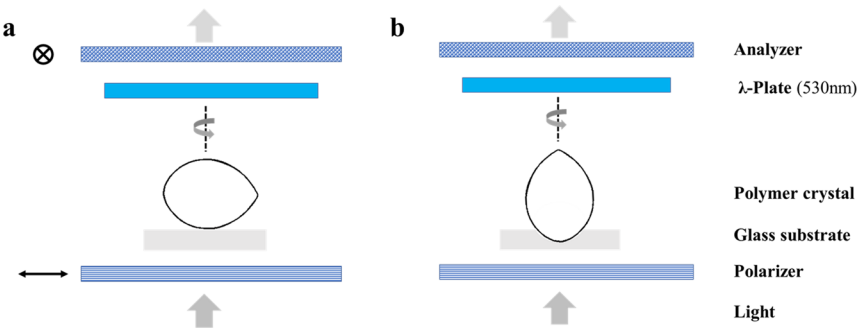


**Figure 1.** Schematic illustration of the polarized optical microscope. The long axis of an anisotropic crystal is parallel to the substrate in (a) and perpendicular in (b). The crystals are rotated in a stage to show the orientation-dependent birefringence.

interfaces, which supplements conventional understanding of polymer crystallization in bulk. The protocols established in this study are potentially useful for creating optical microdevices,[1] encapsulation and delivery,[30−32] and synthesis of anisotropic semicrystalline materials in liquid drops.[33−36]

## METHODS

**Drop Preparation.** Glass capillary microfluidic devices are made for liquid processing. Circular capillaries, with an outer diameter of 1.00 mm, were heated and pulled to break by a Flaming/Brown micropipette puller machine (model P-97, Sutter Instrument Co.). The tip of the injection tube was polished to 30 $\mu$m by sandpaper. For the collection tube, the outer diameter was polished to 120 $\mu$m. The inner surface of the injection tube was treated in a silane solution (1 wt % (heptadecafluoro-1,1,2,2-tetrahydrodecyl)trimethoxysilane in Novec 7500) for 30 min before use. The collection tube was used directly without chemical treatment. The two circular glass capillaries were inserted into a rectangular glass capillary whose inner size is 1.05 mm. The capillaries were aligned coaxially, and the gap was about 60 $\mu$m between the injection and collection capillaries. Two needles were anchored by epoxy resin for the infusion of an oil fluid and an outer water fluid, respectively. The inner water fluid was injected directly from the circular glass capillary. The inner water fluid was encapsulated by the middle oil fluids and was pinched off at the tip of the injection tube by the outer fluid to produce water-in-oil-in-water (W/O/W) drops. In the microfluidic experiment, the infusion rates of three fluids were controlled by three syringe pumps (Harvard Apparatus). The drop-making process was monitored by a high-speed camera (Phantom V9.0), which is affiliated to an inverted microscope.

A 5 wt % poly(vinyl alcohol) (PVA; 13−23 kg/mol, 87−89% hydrolyzed, Sigma-Aldrich) solution was used in the inner and outer aqueous solutions. The middle oil fluid was the 10 wt % poly(L-lactic acid) (PLLA; 50 kg/mol, Sigma-Aldrich) solution in dichloromethane (DCM). Nile red (Sigma-Aldrich), a fluorescent dye, was added at 0.01 mg/mL to assist imaging by a confocal optical microscope (Leica TCS SP5). The fluorescence was excited at 543 nm and was collected from 570 to 660 nm. The other polymers used in the experiment were as follows: poly(D-lactic acid) (PDLA; inherent viscosity of ∼1.2 dL/g, Sigma-Aldrich), poly(D, L-lactic acid) (PLA; 20 kg/mol, Sigma-Aldrich), polycaprolactone (PCL; 45 kg/mol, Sigma-Aldrich), polycaprolactone-*b*-poly(ethylene oxide) (PCL-PEO; PCL block: 25 kg/mol and PEO block: 5 kg/mol, Sigma-Aldrich).

**Solvent Evaporation.** We found that there are two key factors that determine the solvent evaporation rate: one is the volume ratio of the outflow to the collection fluid, and the other is the surface area between air and the collection fluid. The former controls the dissolved DCM concentration in the collection fluid, and the latter controls the evaporation of DCM from the collection fluid to air. To make DCM evaporate quickly ($t < 10^2$ s), 0.1 mL of outflow from a microfluidic device was collected in 1 mL of PVA solution in a plastic Petri dish (35 mm in diameter, lid open). To decrease the DCM evaporation time ($10^2 < t < 10^3$ s), 0.1−0.3 mL of outflow was collected in 1 mL of PVA solution in a plastic Petri dish (35 mm outer diameter, lid open). To make the DCM evaporation time even slower ($10^3 < t < 10^4$ s), 0.3−0.5 mL of outflow was collected in 1 mL of PVA solution in a plastic Petri dish (35 mm in diameter, lid closed). To make the DCM evaporation time very long ($t > 10^4$ s), 0.3−0.5 mL of outflow was collected in 1 mL of PVA solution in a glass vial (1.8 mL capacity, 12 mm outer diameter, lid closed).

**Optical Microscopy.** The polarized optical microscope (POM), Olympus BX53, was used to characterize the crystal birefringence (shown in Figure 1). The polarizer was perpendicularly placed to the analyzer. A $\lambda$ plate, with a featured wavelength of 530 nm, was used to judge the positive or negative birefringence of the spherulites. The $\lambda$ plate is 45° to the polarizer and analyzer. An anisotropic crystal structure can be observed in different axes on a rotation stage. For negative spherulites, the path difference in quadrants I and III was decreased, showing an orange color, while the path difference in quadrants II and IV was enlarged, showing a blue color. The positive spherulites exhibit an opposite property. The isotropic region shows a purple color.

**Scanning Electron Microscopy.** The crystallized particles were first washed by water for several times and then lyophilized to completely remove water. The crystal structures were maintained intact after lyophilization. Samples were further coated by platinum before observation under a scanning electron microscope (JEOL JSM 6700F).

## RESULTS AND DISCUSSION

We use a biodegradable semicrystalline polymer, poly(L-lactic acid) (PLLA), to demonstrate the experimental design. The PLLA is dissolved in dichloromethane (DCM) as the oil phase. The water-in-oil-in-water (W/O/W) liquid drops are prepared using the standard glass capillary devices (Figure 2a).[37] As DCM dissolves in water and evaporates, the PLLA solution gets concentrated and reaches an oversaturated state. This period of time is defined as the solvent evaporation stage. Polymer crystallization is possible to occur from the oversaturated solution by nucleation and growth. This period is defined as the polymer crystallization stage. The solvent evaporation time ($t$) determines the solidified structures in the shell.

When the solvent is eliminated very quickly ($t < 10^2$ s; Figure 2b), the PLLA molecules vitrify in the amorphous state due to significantly decreased molecular motion, and both nucleation and crystal growth are prohibited. The shell is spherical and transparent. When the solvent evaporates slowly, the evaporation time is prolonged ($10^2 < t < 10^4$ s; Figure 2c) and followed by a short crystallization period (∼10s). The nucleation rate is high, and a large number of nuclei are created in this condition. The shell still maintains the spherical shape with many crystallized grain boundaries. When the solvent evaporates more slowly ($10^3 < t < 10^4$ s; Figure 2d), the


https://dx.doi.org/10.1021/acsami.9b17308
ACS Appl. Mater. Interfaces XXXX, XXX, XXX−XXX

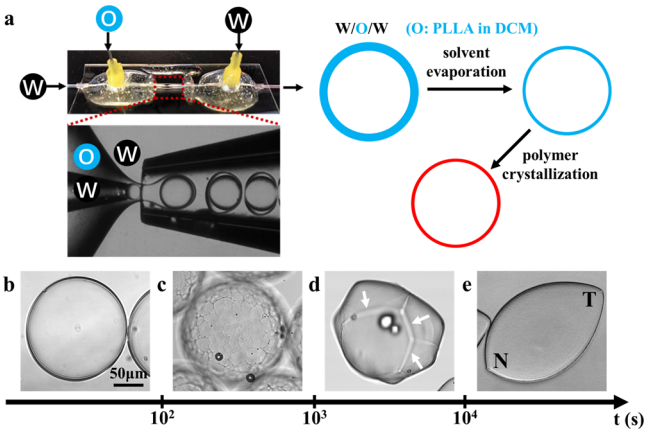


**Figure 2.** Solvent evaporation-induced crystallization in the shell. (a) Transition from liquid drops to crystallized polymer shells by solvent evaporation. (b) Spherical shell without crystallization. (c) Spherical shell with many crystallized grain boundaries. (d) Irregular shell with several crystallized grain boundaries. (e) Anisotropic shell with only one hollow spherulite. Arrows in (d) indicate boundary lines between crystals.

nucleation rate decreases, and the shell becomes irregular with only a few crystallized grain boundaries. The nucleation sites show significantly bent curvature. When the evaporation time is very long ($t > 10^4$ s; Figure 2e), the nucleation rate in a saturated polymer solution is very low, and only one nucleus is created in a long period of time. In this condition, one anisotropic hollow spherulite is developed at the interface of liquid drops. Distinct from a conventional spherulite, this anisotropic hollow spherulite has dipoles: one is the nucleation site ($N$) where the spherulite starts growing, and the other is the termination site ($T$) where the spherulite stops growing.

When more than one nucleus grows in the shell, there are boundaries between adjacent crystallized grains, forming macroscopic defects (arrows in Figure 2d). The more crystals there are, the more the defects (Figure 2c). In contrast, when only one anisotropic hollow spherulite grows in the shell, the impingement of the crystal front converges to the point $T$ (Figure 2e). This anisotropic crystal structure does not have macroscopic defects (such as boundary contact lines or walls or macroscopic voids) that usually appear in colloidal crystals or in polymer crystals grown on plane substrates.[25−27] In addition, the growth dynamics reveals that the creation of an anisotropic crystal occurs spontaneously, unnecessary of any physical or chemical treatments. The details are revealed in Figure 3 and Movie S1.

The crystallization starts from the nucleation site $N$ and propagates in the shell until the growth front converges to the termination site $T$. The contrast is small in the bright-field images (Figure 3a). To enhance the contrast, a fluorescent dye (Nile red) is added in the polymer solution (Figure 3b). During crystallization, the molecular chains of PLLA are added to the growth front, and meanwhile, the dye molecules are repelled from the crystallized region.[12] The dye molecules get more and more concentrated in the front solution and thus show stronger intensity in the shell. By this method, the contour radius of the hollow spherulite, which is the length from the nucleation site to the growth front along the shell, can be precisely measured. The contour lengths are indicated by white dotted lines in Figure 3b and are plotted versus time in Figure 3c. The linear relationship indicates that the growth front propagates at a constant rate (22.5 $\mu$m/min) in the shell. We further define the distance between the nucleation site and termination site as the long axis, $l$, and the largest distance perpendicular to $l$ as the short axis, $s$. Then, the shape

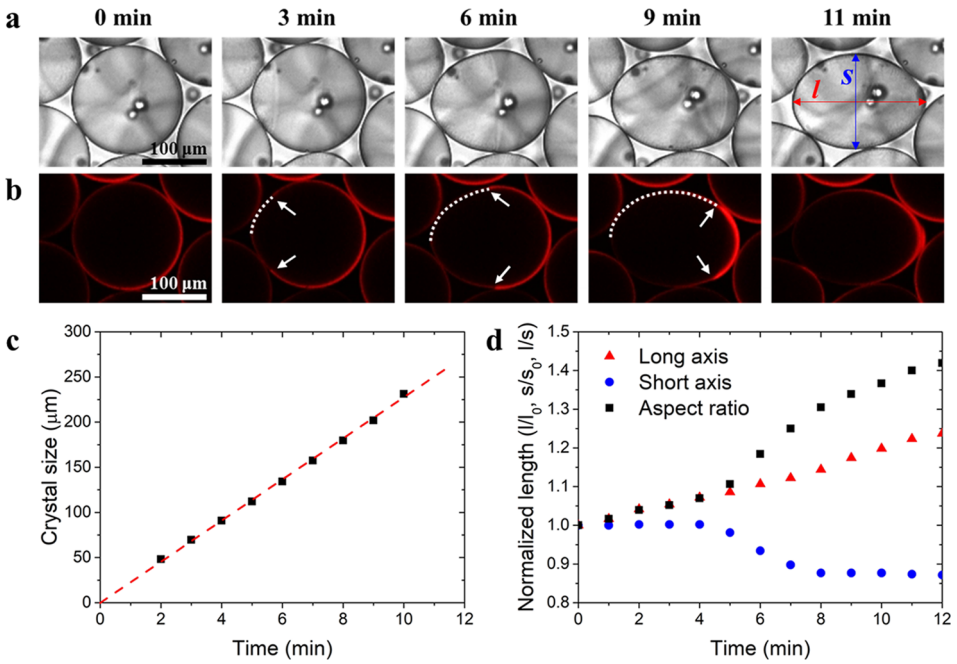


**Figure 3.** Growth dynamics of the anisotropic hollow spherulite. (a) Crystal growth under bright field (b) Fluorescence images. (c) Growth of crystal size with time. (d) Evolution of the normalized long axis, short axis, and aspect ratio with time. The white dotted line in (b) indicates the contour length from the nucleation site to the growth front in the shell. At $t$ = 1 min, the crystal was very small; at $t$ = 11 min, the shell rotated slightly so that the nucleation site is out of focus. So, the contour lengths cannot be precisely measured in these two cases, and the data are not shown in (c).


https://dx.doi.org/10.1021/acsami.9b17308
ACS Appl. Mater. Interfaces XXXX, XXX, XXX−XXX

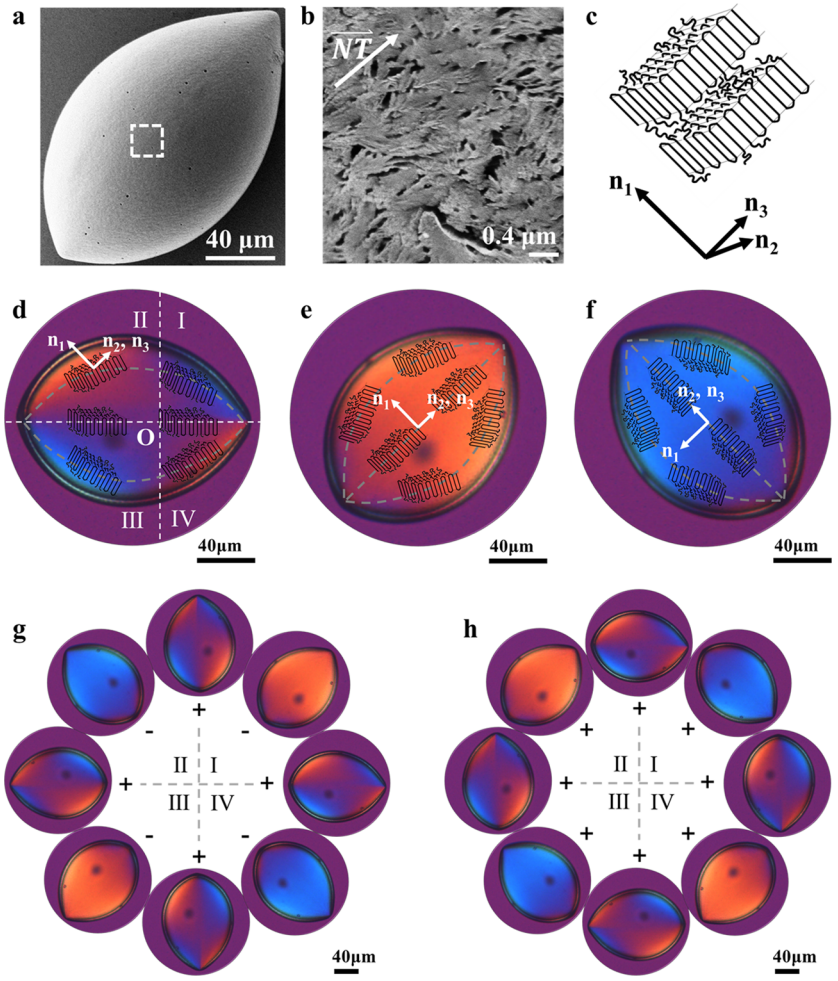


**Figure 4.** Optical properties of the anisotropic hollow spherulite. (a) SEM image. (b) Orientation of lamellar crystals in the long axis. (c) Lamellar crystal and the refractive indices in three directions. (d–f) Orientation-dependent optical behaviors. (g) Alternation of positive/negative birefringence when the long axis is rotated. (h) Alternation of positive/positive birefringence when the short axis is rotated.

anisotropy of the drop is defined by the aspect ratio ($l/s$). The shell is elongated in the long axis and compressed in the short axis (Figure 3d), which leads to the significant increase in the aspect ratio.

The anisotropic hollow spherulite is constituted by smaller crystal units, lamellar sheets (Figure 4a,b). During the crystallization process, random coils fold back and forth to the crystal lattices. The thickness of a crystallized lamellar sheet is limited by the folding of polymer chains, while the sizes in the other two dimensions are not limited. Those lamellae align in the long axis from the nucleation site to the termination site ($\overrightarrow{NT}$). It should be noted that the refractive index of a lamellar crystal is large in the thickness direction ($n_1$ = 1.55) and smaller in the other two directions ($n_2$ = 1.45 and $n_3$ = 1.46),[7] which is the basis of optical anisotropy (Figure 4c).

The alignment of the lamellar crystals endows the anisotropic hollow spherulite with remarkable orientation-sensitive optical properties. The optical birefringence is observed between a polarizer and a crossed analyzer. A $\lambda$ plate with a wavelength of 530 nm is inserted in between. When the anisotropic hollow spherulite is rotated with respect to the geometric center, it shows noncentrosymmetric, orientation-sensitive birefringence (Figure 1a and Movie S2).

Here, we show the birefringence of the anisotropic hollow spherulite at three typical positions (Figure 4d–f). When the long axis is in the horizontal direction, the spherulite presents a blue color in quadrants I and III and an orange color in quadrants II and IV, with respect to the optical center $O$ (Figure 4d). The refractive index is larger in the radial direction (mainly contributed by $n_1$) than that in the tangential direction (mainly contributed by $n_2$ and $n_3$). In this case, the spherulite behaves positive birefringence. When the long axis is rotated by 45° azimuthally (Figure 4e), there is an orange color. When the long axis is tilted by 135° (Figure 4f), there is a blue color. The positive (+) or negative (−) nature of the spherulite in the latter two cases is not straightforward to identify, which depends on the reference point.

When the long axis is rotated in plane with respect to point $N$ (Figure 4g), a large refractive index in the tangential direction leads to negative birefringence, showing an orange color in quadrants I and III and a blue color in quadrants II and IV. Thus, there is alternation of +/− birefringence in the rotation plane. In comparison, when the short axis is rotated (Figure 4h), the refractive index is always large in the radial direction, which indicates the positive nature of birefringence. There is alternation of +/+ birefringence during rotation.

Because of the anisotropic shape, the long axis of the hollow spherulite prefers lying parallel to the substrate, as shown in Figures 1a and 4. There is also an unfavorable orientation when the long axis is perpendicular to the substrate (Figure 1b


https://dx.doi.org/10.1021/acsami.9b17308
ACS Appl. Mater. Interfaces XXXX, XXX, XXX−XXX

and Movie S3). With respect to the center $N$ (or $T$) in the projected image, the lamellae spread (or converge) in the radial direction. The hollow spherulite presents negative birefringence because the refractive index is always larger in the tangential direction than that in the radial direction (Figure 5a). The rotational centrosymmetry results in orientation-insensitive, negative birefringence during rotation (Figure 5b).

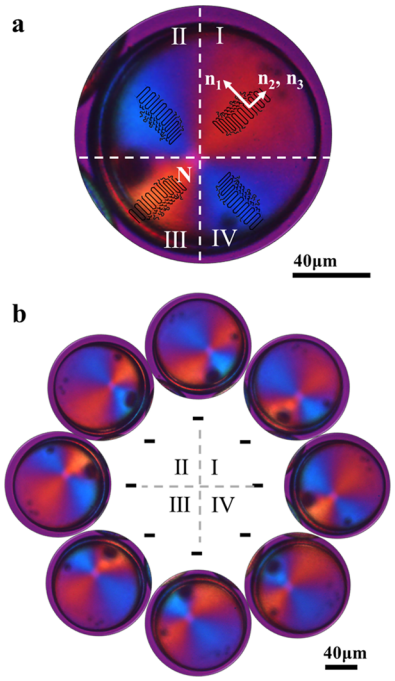


**Figure 5.** Negative birefringence of the anisotropic hollow spherulite with the long axis perpendicular to the substrate. Lamellar orientation is illustrated in (a). The orientation-insensitive negative birefringence is revealed in (b).

It should be noted that the centrosymmetric configuration in Figure 5 shares the same birefringent properties with conventional spherulites crystallized in bulk (Figure S1). The crystallinity of spherulites from liquid drops is about 47.5%, relatively lower than that from bulk (Figure S2a).[38] However, the crystallization from liquid drops adopts the $\alpha$-form crystal type, which is also the same with conventional spherulites that are thermally annealed at a high temperature (Figure S2b).[39] So, the fascinating optical birefringence reported in this study is determined by the anisotropic shell structure, not due to any change of the crystal type.

Based on the experiments above, a superior advantage of these anisotropic hollow spherulites is that they provide the positive or negative birefringence as long as they are properly orientated. The key factor is that macroscopic defects are vanished during crystal growth. For comparison, hollow spherulites with macroscopic defects (i.e., boundary effect, shown in Figure S3) are detrimental to the birefringent behavior.

Although the anisotropic hollow spherulite is developed spontaneously during crystallization, we can further tune the aspect ratio by applying osmotic pressure (Figure 6). The osmotic pressure is mediated by the concentration of sucrose between the inner and the outer fluids. For example, when there is $x$ M sucrose ($0 \leq x \leq 1$) inside the drop and 1.0 M sucrose outside, the osmotic pressure applied to the shell is

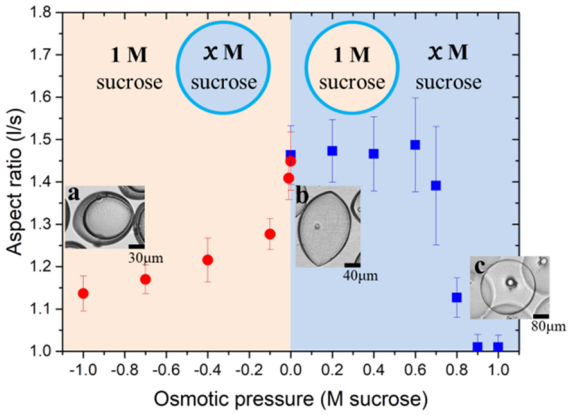


**Figure 6.** Modulation of the aspect ratio by osmotic pressure. (a) Slightly anisotropic hollow spherulite when the osmotic pressure is equivalent to −1.0 M sucrose. (b) Highly anisotropic hollow spherulite when the osmotic pressure is balanced at 0. (c) Spherical crystallized shell when the osmotic pressure is 1.0 M sucrose.

equivalent to $(x-1)$ M sucrose. The deformation is very sensitive to the osmotic pressure, and the aspect ratio decreases quickly with osmotic pressure. However, this compressive pressure leads to thickening of the shell and cannot drive the shell into the spherical shape even when the osmotic pressure is as large as −1.0 M sucrose (Figure 6a). In the opposite case, we apply an osmotic pressure with $(1-x)$ M sucrose, that is, 1.0 M sucrose inside the drop and $x$ M sucrose outside. The aspect ratio maintains at ∼1.5 (Figure 6b) until the pressure is larger than 0.7, and spherical shells are obtained when the osmotic pressure is over 0.8 (Figure 6c). This set of experiment provides a facile method to tune the shape anisotropy with an aspect ratio from 1 to 1.5, simply by applying different osmotic pressures. As shown in Figures 4 and 5, the orientation-dependent birefringence is strongly correlated with the anisotropy of the crystallized structure in the shell. So, the optical properties can also be modulated by tuning aspect ratios of the shell with osmotic pressure.

It is well known that isotropic interfacial tension maintains a liquid drop in spherical shape. The above experiments indicate that the crystallization in the shell generates anisotropy spontaneously, which dominates over the interfacial tension. From the perspective of energy analysis, as a crystal is growing on a spherical shell, there is a cumulative increase in elastic energy because of crystal bending with a curvature. The elastic energy of a 2D crystal (very thin, radius of $r$) on a sphere (radius of $R$) is proportional to $\sim Er^6/R^4$.[26] $E$ is the Young's modulus, which is typically $\sim 10^9$ Pa for most polymer crystals. The elastic energy vanishes on a plane surface ($R$ is infinity) and is significant as crystal size increases or the drop size decreases. The surface energy scales to $\sim \gamma r$[26] where $\gamma$ is the line tension and is $\sim 10^{-2}$ N/m for most polymer interfaces. For the hollow spherulite grown on a microdroplet in this study, the surface energy is definitely very small, compared with the elastic energy. As there is significant increase in elastic energy with the crystal size, the elastic energy is typically released in two ways. One is to maintain the spherical shape but to create defects or voids. Polymer single crystals are found defective in miniemulsions,[23,24] and colloidal crystals on microdroplets generate macroscopic voids spontaneously.[25−27] We indeed observed voids on the scale of nanometers (Figure 4b), but macroscopic voids are absent in the shell, which is not detrimental to macroscopic optical properties. The other way


https://dx.doi.org/10.1021/acsami.9b17308
ACS Appl. Mater. Interfaces XXXX, XXX, XXX−XXX

is to deform the shell shape to dissipate elastic energy spontaneously. As indicated in Figure 3, the shell envelope deforms upon crystallization, which indicates that the elastic energy is concentrated near the nucleation site. Dissipation of elastic energy drives the anisotropic growth of the shell. To maintain the spherical shape during crystallization, the osmotic pressure needs to be sufficiently high, which provides an isotropic stress to overcome the nonuniformly distributed elastic energy.

Similar to our finding in polymer crystallization, there are reports on spindle-like drops of liquid crystals (LC), namely, tactoids, which are driven by elastic deformation of LC molecules in a long range.[40,41] However, the differences between tactoids and anisotropic hollow spherulites are significant. The dipoles in tactoids are two +1 disclination defects (or split into four +1/2 disclination defects at most). For polymer crystallization in this study, the dipole includes a nucleation site and a termination site. The number of nucleation sites is not limited and could be easily tuned by experimental conditions. Moreover, the spatial distribution of LC molecules follows the bipolar director field, which creates a spindle shape for small drops (usually smaller than ~1 $\mu$m) and transforms to a radial director field, which creates a spherical shape for large drops. So, it is difficult to create large anisotropic tactoids, while anisotropic hollow spherulites are created on tens to hundreds of micrometers in this study.

Although the anisotropic PLLA hollow spherulites are presented in this study as an example, the idea shows generality in other semicrystalline systems, including typical biodegradable semicrystalline polymers (the anisotropic hollow spherulites of poly(D-lactic acid) (PDLA) and polycaprolactone (PCL) are shown in Figures S4 and S5, respectively), the mixtures of semicrystalline and amorphous polymers (crystallization of PLLA in the PLLA/PLA mixture is shown in Figure S6, for example), and semicrystalline polymers with amphiphilic surfactants (crystallization of PCL with polycaprolactone-*b*-poly(ethylene oxide) as a surfactant is shown in Figure S7, for example). All the systems show the spontaneous formation of anisotropic hollow spherulites, irrespective of molecular chirality, chemical constitution, or interfacial modification. The general phenomena indicate that semicrystalline polymers, the largest species in the polymer family, are able to provide orientation-sensitive optical birefringence when they grow in an anisotropic shape under appropriate conditions. There are still open questions left at the current stage. We notice that the anisotropic shape is distinct from polymer to polymer. The mechanical origin of elastic energy might be determined by the microscopic properties of crystallized structures, such as crystal type, crystallinity, etc., which will be systematically studied in future work.

## CONCLUSIONS

We use a semicrystalline polymer PLLA as a model to illustrate the anisotropic crystal growth at interfaces of liquid drops. The nucleation density and macroscopic defects can be well controlled in the crystallization process. When only one nucleus is initiated, the drop is deformed spontaneously into an anisotropic hollow spherulite with dipoles, which exhibits noncentrosymmetric, orientation-sensitive birefringent properties. The aspect ratio of the anisotropic hollow spherulite can be easily mediated by applied osmotic pressure. The generality of our work indicates that a broad class of semicrystalline polymers can be engineered with well-controlled anisotropic shape, defect, and orientation-sensitive optical properties, which are useful for developing optical microdevices, drug carriers, and the synthesis of anisotropic microparticles in emulsion drops.

## ASSOCIATED CONTENT

### Supporting Information

The Supporting Information is available free of charge at https://pubs.acs.org/doi/10.1021/acsami.9b17308.

(Part A) Negative PLLA spherulites crystallized in bulk, (Part B) DSC and WAXS data for PLLA spherulites crystallized in droplets and in bulk, (Part C) irregular birefringence with significant boundary effect, (Part D) anisotropic hollow spherulites of poly(D-lactic acid), (Part E) anisotropic hollow spherulites of polycaprolactone, (Part F) anisotropic hollow spherulites of a PLLA/PLA mixture, and (Part G) anisotropic hollow spherulites of PCL with PCL-PEO as a surfactant (PDF)

Movie S1: Tracking the anisotropic hollow spherulite growth by a confocal optical microscope (MP4)

Movie S2: Noncentrosymmetric, orientation-sensitive birefringence of the PLLA hollow spherulite with the long axis parallel to the substrate (MP4)

Movie S3: Negative birefringence of the PLLA hollow spherulite with the long axis perpendicular to the substrate (MP4)

## AUTHOR INFORMATION


### Corresponding Author

**Weichao Shi** − *Nankai University, Tianjin, China;* orcid.org/0000-0003-4625-4797; Email: weichaoshi@nankai.edu.cn

### Other Authors

**Xiaotong Chen** − *Nankai University, Tianjin, China*

**Baihui Li** − *Nankai University, Tianjin, China*

**David A. Weitz** − *Harvard University, Cambridge, Massachusetts;* orcid.org/0000-0001-6678-5208

Complete contact information is available at: https://pubs.acs.org/10.1021/acsami.9b17308


### Notes

The authors declare no competing financial interest.

## ACKNOWLEDGMENTS

W.S. is grateful to the funding support from the Nankai University and National Natural Science Foundation of China (no. 21973050). This work is dedicated to the 100th anniversary of Nankai University.

## REFERENCES

(1) Goodling, A. E.; Nagelberg, S.; Kaehr, B.; Meredith, C. H.; Cheon, S. I.; Saunders, A. P.; Kolle, M.; Zarzar, L. D. Colouration by Total Internal Reflection and Interference at Microscale Concave Interfaces. *Nature* **2019**, *566*, 523−527.

(2) Mashkour, M.; Kimura, T.; Mashkour, M.; Kimura, F.; Tajvidi, M. Printing Birefringent Figures by Surface Tension-Directed Self-Assembly of a Cellulose Nanocrystal/Polymer Ink Components. *ACS Appl. Mater. Interfaces* **2019**, *11*, 1538−1545.

(3) Fenzl, C.; Hirsch, T.; Wolfbeis, O. S. Photonic Crystals for Chemical Sensing and Biosensing. *Angew. Chem., Int. Ed.* **2014**, *53*, 3318−3335.

(4) Zhao, Y.; Xie, Z.; Gu, H.; Zhu, C.; Gu, Z. Bio-Inspired Variable Structural Color Materials. *Chem. Soc. Rev.* **2012**, *41*, 3297−3317.
(5) Wang, M.; Zhao, C.; Miao, X.; Zhao, Y.; Rufo, J.; Liu, Y. J.; Huang, T. J.; Zheng, Y. Plasmofluidics: Merging Light and Fluids at the Micro-/Nanoscale. *Small* **2015**, *11*, 4423−4444.
(6) Lotz, B.; Miyoshi, T.; Cheng, S. Z. D. 50th Anniversary Perspective: Polymer Crystals and Crystallization: Personal Journeys in a Challenging Research Field. *Macromolecules* **2017**, *50*, 5995−6025.
(7) Ye, H.-M.; Xu, J.; Freudenthal, J.; Kahr, B. On the Circular Birefringence of Polycrystalline Polymers: Polylactide. *J. Am. Chem. Soc.* **2011**, *133*, 13848−13851.
(8) Keller, A. The Spherulitic Structure of Crystalline Polymers. Part I. Investigations with the Polarizing Microscope. *J. Polym. Sci.* **1955**, *17*, 291−308.
(9) Keller, A. The Spherulitic Structure of Crystalline Polymers. Part II. The Problem of Molecular Orientation in Polymer Spherulites. *J. Polym. Sci.* **1955**, *17*, 351−364.
(10) Yu, H.; Kobayashi, T. Fabrication of Stable Nanocylinder Arrays in Highly Birefringent Films of an Amphiphilic Liquid-Crystalline Diblock Copolymer. *ACS Appl. Mater. Interfaces* **2009**, *1*, 2755−2762.
(11) Crist, B.; Schultz, J. M. Polymer Spherulites: A Critical Review. *Prog. Polym. Sci.* **2016**, *56*, 1−63.
(12) Shi, W.; Han, C. C. Dynamic Competition between Crystallization and Phase Separation at the Growth Interface of a PMMA/PEO Blend. *Macromolecules* **2012**, *45*, 336−346.
(13) Shi, W.; Yang, J.; Zhang, Y.; Luo, J.; Liang, Y.; Han, C. C. Lamellar Orientation Inversion under Dynamic Interplay between Crystallization and Phase Separation. *Macromolecules* **2012**, *45*, 941−950.
(14) Wunderlich, B. Crystal Structure, Morphology, Defects. In *Macromolecular Physics*; Vol. *1*; Academic Press: 1973.
(15) Du, J.; O'reilly, R. K. Anisotropic Particles with Patchy, Multicompartment and Janus Architectures: Preparation and Application. *Chem. Soc. Rev.* **2011**, *40*, 2402−2416.
(16) Millman, J. R.; Bhatt, K. H.; Prevo, B. G.; Velev, O. D. Anisotropic Particle Synthesis in Dielectrophoretically Controlled Microdroplet Reactors. *Nat. Mater.* **2005**, *4*, 98−102.
(17) Liebi, M.; Kuster, S.; Kohlbrecher, J.; Ishikawa, T.; Fischer, P.; Walde, P.; Windhab, E. J. Magnetically Enhanced Bicelles Delivering Switchable Anisotropy in Optical Gels. *ACS Appl. Mater. Interfaces* **2014**, *6*, 1100−1105.
(18) Metselaar, L.; Dozov, I.; Antonova, K.; Belamie, E.; Davidson, P.; Yeomans, J. M.; Doostmohammadi, A. Electric-Field-Induced Shape Transition of Nematic Tactoids. *Phys. Rev. E* **2017**, *96*, 022706.
(19) Jang, S. G.; Audus, D. J.; Klinger, D.; Krogstad, D. V.; Kim, B. J.; Cameron, A.; Kim, S.-W.; Delaney, K. T.; Hur, S.-M.; Killops, K. L.; Fredrickson, G. H.; Kramer, E. J.; Hawker, C. J. Striped, Ellipsoidal Particles by Controlled Assembly of Diblock Copolymers. *J. Am. Chem. Soc.* **2013**, *135*, 6649−6657.
(20) Klinger, D.; Wang, C. X.; Connal, L. A.; Audus, D. J.; Jang, S. G.; Kraemer, S.; Killops, K. L.; Fredrickson, G. H.; Kramer, E. J.; Hawker, C. J. A Facile Synthesis of Dynamic, Shape-Changing Polymer Particles. *Angew. Chem., Int. Ed.* **2014**, *53*, 7018−7022.
(21) Zhu, J.; Hayward, R. C. Hierarchically Structured Microparticles Formed by Interfacial Instabilities of Emulsion Droplets Containing Amphiphilic Block Copolymers. *Angew. Chem., Int. Ed.* **2008**, *47*, 2113−2116.
(22) Zhu, J.; Hayward, R. C. Spontaneous Generation of Amphiphilic Block Copolymer Micelles with Multiple Morphologies through Interfacial Instabilities. *J. Am. Chem. Soc.* **2008**, *130*, 7496−7502.
(23) Wang, W.; Qi, H.; Zhou, T.; Mei, S.; Han, L.; Higuchi, T.; Jinnai, H.; Li, C. Y. Highly Robust Crystalsome via Directed Polymer Crystallization at Curved Liquid/Liquid Interface. *Nat. Commun.* **2016**, *7*, 10599.
(24) Staub, M. C.; Li, C. Y. Confined and Directed Polymer Crystallization at Curved Liquid/Liquid Interface. *Macromol. Chem. Phys.* **2018**, *219*, 1700455.
(25) Irvine, W. T. M.; Vitelli, V.; Chaikin, P. M. Pleats in Crystals on Curved Surfaces. *Nature* **2010**, *468*, 947−951.
(26) Meng, G.; Paulose, J.; Nelson, D. R.; Manoharan, V. N. Elastic Instability of a Crystal Growing on a Curved Surface. *Science* **2014**, *343*, 634−637.
(27) Ma, L.; Liu, X.; Soh, A.-K.; He, L.; Wu, C.; Ni, Y. Growth of Curved Crystals: Competition between Topological Defect Nucleation and Boundary Branching. *Soft Matter* **2019**, *15*, 4391−4400.
(28) Liang, H.-L.; Schymura, S.; Rudquist, P.; Lagerwall, J. Nematic-Smectic Transition under Confinement in Liquid Crystalline Colloidal Shells. *Phys. Rev. Lett.* **2011**, *106*, 247801.
(29) Shin, H.; Bowick, M. J.; Xing, X. Topological Defects in Spherical Nematics. *Phys. Rev. Lett.* **2008**, *101*, 037802.
(30) Kim, S.-H.; Shum, H. C.; Kim, J. W.; Cho, J.-C.; Weitz, D. A. Multiple Polymersomes for Programmed Release of Multiple Components. *J. Am. Chem. Soc.* **2011**, *133*, 15165−15171.
(31) Nam, C.; Yoon, J.; Ryu, S. A.; Choi, C.-H.; Lee, H. Water and Oil Insoluble PEGDA-Based Microcapsule: Biocompatible and Multicomponent Encapsulation. *ACS Appl. Mater. Interfaces* **2018**, *10*, 40366−40371.
(32) Lee, H.; Choi, C.-H.; Abbaspourrad, A.; Wesner, C.; Caggioni, M.; Zhu, T.; Weitz, D. A. Encapsulation and Enhanced Retention of Fragrance in Polymer Microcapsules. *ACS Appl. Mater. Interfaces* **2016**, *8*, 4007−4013.
(33) Piradashvili, K.; Alexandrino, E. M.; Wurm, F. R.; Landfester, K. Reactions and Polymerizations at the Liquid-Liquid Interface. *Chem. Rev.* **2016**, *116*, 2141−2169.
(34) Song, H.; Chen, D. L.; Ismagilov, R. F. Reactions in Droplets in Microfluidic Channels. *Angew. Chem. Int. Ed.* **2006**, *45*, 7336−7356.
(35) Nuraje, N.; Su, K.; Yang, N.-L.; Matsui, H. Liquid/Liquid Interfacial Polymerization to Grow Single Crystalline Nanoneedles of Various Conducting Polymers. *ACS Nano* **2008**, *2*, 502−506.
(36) Liu, X.; Yi, Q.; Han, Y.; Liang, Z.; Shen, C.; Zhou, Z.; Sun, J. L.; Li, Y.; Du, W.; Cao, R. A Robust Microfluidic Device for the Synthesis and Crystal Growth of Organometallic Polymers with Highly Organized Structures. *Angew. Chem. Int. Ed.* **2015**, *54*, 1846−1850.
(37) Shi, W.; Didier, J. E.; Ingber, D. E.; Weitz, D. A. Collective Shape Actuation of Polymer Double Emulsions by Solvent Evaporation. *ACS Appl. Mater. Interfaces* **2018**, *10*, 31865−31869.
(38) Tsuji, H.; Miyauchi, S. Poly (L-lactide): VI Effects of Crystallinity on Enzymatic Hydrolysis of Poly (L-lactide) Without Free Amorphous Region. *Polym. Degrad. Stab.* **2001**, *71*, 415−424.
(39) Kobayashi, J.; Asahi, T.; Ichiki, M.; Oikawa, A.; Suzuki, H.; Watanabe, T.; Fukada, E.; Shikinami, Y. Structural and Optical Properties of Poly Lactic Acids. *J. Appl. Phys.* **1995**, *77*, 2957−2973.
(40) Verhoeff, A. A.; Bakelaar, I. A.; Otten, R. H. J.; van der Schoot, P.; Lekkerkerker, H. N. W. Tactoids of Plate-Like Particles: Size, Shape, and Director Field. *Langmuir* **2011**, *27*, 116−125.
(41) Wang, P.-X.; MacLachlan, M. J. Liquid Crystalline Tactoids: Ordered Structure, Defective Coalescence and Evolution in Confined Geometries. *Philos. Trans. R. Soc., A* **2017**, *376*, 20170042.


https://dx.doi.org/10.1021/acsami.9b17308
*ACS Appl. Mater. Interfaces* XXXX, XXX, XXX−XXX